7132 J. Med. Chem. 2009, 52, 7132–7141
DOI: 10.1021/jm9011388

Journal of Medicinal Chemistry Article

Design of HIV Protease Inhibitors Based on Inorganic Polyhedral Metallacarboranes†

Pavlína Řezáčová,*[,‡,§] Jana Pokorná,[‡,∥] Jiří Brynda,[‡,§] Milan Kožíšek,[‡,∥] Petr Cígler,[‡,⊥] Martin Lepšík,[‡] Jindřich Fanfrlík,[‡] Jan Řezáč,[‡] Klára Grantz Šašková,[‡,∥] Irena Sieglová,[‡,§] Jaromír Plešek,[#] Václav Šícha,[#] Bohumír Grüner,[#] Heike Oberwinkler,[▽] Juraj Sedláček',[§] Hans-Georg Kräusslich,[▽] Pavel Hobza,[‡] Vladimír Král,[⊥] and Jan Konvalinka[‡,§,∥]

[‡]*Institute of Organic Chemistry and Biochemistry, Academy of Sciences of the Czech Republic, v.v.i., Gilead Sciences and IOCB Research Center, Flemingovo nam. 2, 16610 Praha 6, Czech Republic,* [§]*Institute of Molecular Genetics, Academy of Sciences of the Czech Republic v.v.i., Flemingovo nam. 2, 166 10 Praha 6, Czech Republic,* [∥]*Department of Biochemistry, Faculty of Science, Charles University, Hlavova 8, 128 43 Praha 2, Czech Republic,* [⊥]*Department of Analytical Chemistry, Institute of Chemical Technology, Technická 5, 166 28 Praha 6, Czech Republic,* [#]*Institute of Inorganic Chemistry, Academy of Sciences of the Czech Republic, v.v.i., Area of Research Institutes 1001, 250 68 Husinec-Řež u Prahy, Czech Republic, and* [▽]*Department of Virology, University of Heidelberg, Im Neuenheimer Feld 324, D-69120 Heidelberg, Germany*

Received July 31, 2009

HIV protease (HIV PR) is a primary target for anti-HIV drug design. We have previously identified and characterized substituted metallacarboranes as a new class of HIV protease inhibitors. In a structure-guided drug design effort, we connected the two cobalt bis(dicarbollide) clusters with a linker to substituted ammonium group and obtained a set of compounds based on a lead formula $[H_2N\text{-}(8\text{-}(C_2H_4O)_2\text{-}1,2\text{-}C_2B_9H_{10})(1',2'\text{-}C_2B_9H_{11})\text{-}3,3'\text{-}Co)_2]Na$. We explored inhibition properties of these compounds with various substitutions, determined the HIV PR:inhibitor crystal structure, and computationally explored the conformational space of the linker. Our results prove the capacity of linker-substituted dual-cage cobalt bis(dicarbollides) as lead compounds for design of more potent inhibitors of HIV PR.

Introduction

The human immunodeficiency virus protease (HIV PR[a]), an enzyme belonging to the aspartic protease family, is responsible for cleavage of the Gag and Gag-Pol polyprotein precursors necessary for production of infectious viral particles.[1] Since the demonstration that HIV PR plays an essential role in the HIV replication cycle, this enzyme has become one of the primary targets for antiviral drug design leading to the development of hundreds of inhibitory compounds. Nine of these are currently FDA-approved for clinical use and several others are in the pipeline of pharmaceutical companies (reviewed in ref 2). All FDA-approved drugs represent competitive inhibitors that occupy the enzyme active site and share a similar structural scaffold mimicking the peptide substrate. The major problem that limits the therapeutic efficiency of protease inhibitors (PIs) is drug resistance caused by extensive mutations in PR.[3] Development of new inhibitors acting by an alternative mode of inhibition and capable of inhibiting multidrug resistant species is thus essential for the sustained successful treatment of HIV-positive patients.

In our search for novel structural types of unconventional chemical compounds, we have recently identified a group of inorganic carbon/boron (carborane) cluster complexes, namely cobalt bis(dicarbollides), as promising frameworks for nonpeptide PIs.[4] These clusters form icosahedral sandwich complexes of two icosahedral $C_2B_9H_{11}^{2-}$ dicarbollide cages and a central Co^{3+} ion.[5] (Metalla)carborane compounds show remarkable stability originating from delocalized bonding within their triangular boron facets and over the whole cage, a phenomenon referred to as three-dimensional aromaticity.[6,7] The use of boron clusters as hydrophobic pharmacophores have lately been gaining in importance (reviewed in refs 8,9). Specifically, various carboranes were introduced for use in boron neutron capture therapy,[9−11] radioimmunodetection, and radioimmunotherapy.[12,13] Other biologically active carborane derivatives include carborane-based insect neuropeptides, antineoplastic and cytotoxic agents, estrogen agonists and antagonists, retinoids, protein kinase C modulators, and others.[9]

We have shown in our previous works that substituted cobalt bis(dicarbollides) are specific inhibitors of HIV PR[4] and also effective inhibitors of HIV-1 PR variants resistant to clinical inhibitors.[14] The tested compounds showed little toxicity in tissue culture and exhibited substantial chemical and biological stability. The crystal structure of the parent cluster, cobalt bis(1,2-dicarbollide) ion in complex with wild-type HIV-1 PR, revealed a unique binding mode. Two inhibitor molecules occupied in a nonsymmetrical manner symmetric hydrophobic pockets in the flap-proximal region of the S3 and S3′ subsites of the enzyme active site.[4] In a structure-guided drug design effort, we connected the two parent clusters with a linker to yield compounds with significantly increased inhibitory potency toward HIV-1 PR.

In this work, we have designed and synthesized a set of compounds set of double (triple) cluster compounds

†PDB ID: Atomic coordinates and experimental structure factors have been deposited with the Protein Data Bank with the code 3I8W.

*To whom correspondence should be addressed. Phone: + 420220183135. Fax: + 420220183280. E-mail: rezacova@uochb.cas.cz.

[a] Abbreviations: ADP, atomic displacement parameter; FDA; Food and Drug Administration; HIV PR; human immunodeficiency virus protease; K_i, inhibition constant; K_m, Michaelis constant; PI, protease inhibitor; rmsd, root-mean square deviation; QM, quantum mechanics; WT, wild-type.

 Published on Web 10/29/2009

Scheme 1. Synthetic Method Used for Construction of the Anionic Molecules **1**−**10**[a]

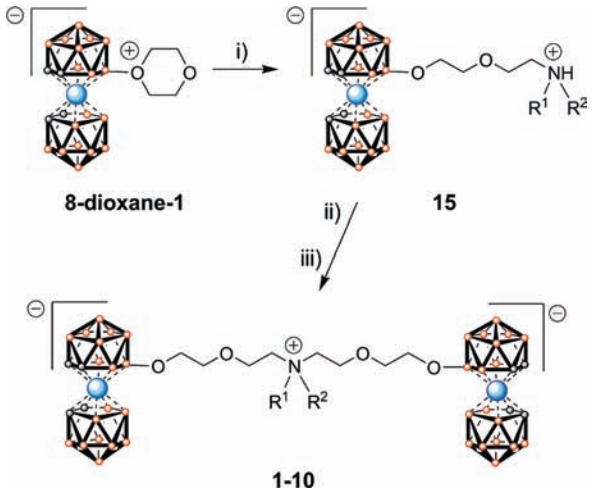

[a] (i) Toluene:ethyleneglycol dimethyl ether (DME) 4:1, 60 °C, 4 h; (ii) NaH, toluene: DME 4: 1, (iii) 8-dioxane-**1**, room temperature.

(Table 1 and Scheme 1) of general formulation $[^1R^2RN\text{-}(8\text{-}(C_2H_4O)_2\text{-}1,2\text{-}C_2B_9H_{10})(1',2'\text{-}C_2B_9H_{11})\text{-}3,3'\text{-}Co)_2]^{n-}$ (where ^1R = H, $-C_2H_5$, $-n\text{-}C_4H_9$, $-C_2H_4OH$, $-t\text{-}C_4H_9$, $-C(CH_2OH)_3$, $-C_3H_6COO^-$, $-C_2H_4SO_3^-$, $-CH_2C_6H_5$, $-SO_2C_6H_5\text{-}3\text{-}CH_3$, $-7\text{-}CB_{10}H_{11}^-$, $-1\text{-}CB_{11}H_{11}$, $-[\mu\text{-}8,8' < (1,2\text{-}C_2B_{10}H_{10})\text{-}3,3'Co]^-$, ^2R = none, H, $-C_2H_5$, n = 1 and 2) (**1**−**13**) or $[n\text{-}C_4H_9\text{-}H_2N\text{-}(10\text{-}(C_2H_4O)_2\text{-}nido\text{-}7,8\text{-}C_2B_9H_{10})_2]^-$ (**14**) and investigated their HIV PR inhibition properties. We have determined the crystal structure of the parental compound $[H_2N\text{-}(8\text{-}(C_2H_4O)_2\text{-}1,2\text{-}C_2B_9H_{10})(1',2'\text{-}C_2B_9H_{11})\text{-}3,3'\text{-}Co)_2]Na$ (designated here **1**) in complex with wild-type HIV-1 PR. As the lack of a continuous electron-density map in the crystal structure suggested numerous possible linker conformations, we explored the conformational space of the linker computationally. This study demonstrates the capacity of linker-substituted dual-cage cobalt bis(dicarbollides) as lead compounds for design of more potent HIV PIs.

Results

Inhibitor Design and Synthesis. The structural formulas of the compounds studied in this work are shown in Table 1. The series involves symmetric molecules designed based on the most effective structures from our previous study.[4] These zwitterionic−anionic molecules contain two or three carborane clusters bonded via an N-substituted bis(ethyleneglycol)amine linker. We focused on the substitution of the central part. In addition to hydrocarbon/functional group substituents, we also used various boron hydride clusters differing distinctively in hydrophobicity and acidity. It should be noted here that the total negative charge of several tested members of the series is increased to −2 due to the presence of the third anionic cluster or due to the substitution pattern.

The selection of synthetic routes was limited to double (triple) ring-opening of the 8-dioxane cobalt-bis(dicarbollide) zwitterion by a variety of organic amines or carborane and metallacarborane building blocks substituted with amine/ammonium functions as shown in Scheme 1 and Table 1.

Compounds containing three boron cages **11**−**13** are also available through this approach if a boron cluster substituted with ammonium function (deprotonated using NaH) is used instead of the organic amine in the first ring-opening step. These synthetic routes are efficient, reliable, and almost quantitative for the majority of compounds presented in this article.

The synthesis of compound **14** was also based on this methodology but using 10-dioxane-*nido*-7,8-$C_2B_9H_{11}$ (**15**) reactive building block instead of **1**. The 11 vertex carborane derivative 155-P has been known for a long time from reactions of the parent *nido*-$[7,8\text{-}C_2B_9H_{12}]^-$ anion with dioxane promoted by formaldehyde/HCl[15] or $HgCl_2$.[16] We report here that the compound 155-P can be obtained more effectively if the neutral *nido*-7,8-$C_2B_9H_{13}$ carborane is heated in toluene in the presence of an excess of dioxane. For details on the synthetic procedures, see the Supporting Information.

Enzyme and Antiviral Inhibition Studies. The inhibitory properties of all compounds were tested in an in vitro spectrophotometric enzyme assay using a chromogenic substrate and recombinant wild-type HIV-1 PR. The results are shown in Table 1. First, the IC_{50} values were measured to screen for inhibition potency. The IC_{50} values in submicromolar range proved the inhibition potency for all dual-cage cobalt bis(dicarbollide) compounds. Significantly higher IC_{50} values for compound **14** provided evidence for the requirement of a bulkier cobalt bis(dicarbollide) moiety for effective inhibition of HIV PR.

Inhibition mechanism was determined using double reciprocal Lineweaver−Burk plot[17] (Figure S1 in Supporting Information). The tested compounds exhibited various inhibition types: competitive, noncompetitive, and for four compounds **2**, **9**, **10**, and **12**, the inhibition mechanism was dependent on the compound concentration (Table 1). At low concentrations, the inhibition mechanism was noncompetitive or mixed, and with the increasing concentration the mechanism shifted toward the competitive mode (Figure S1C in Supporting Information).

For six compounds with competitive mode of inhibition, inhibition constants (K_i values) were determined (Table 1). These values can be directly compared in order to draw conclusions on the relation between compound structure and inhibition efficiency. Connection of the two parental cobalt bis(dicarbollide) clusters with a hydrophilic linker in **1** resulted in an approximately 14-fold improvement of the K_i value compared to value for parent cobalt bis(1,2-dicarbollide) ion.[4] Further improvement of the in vitro inhibitory potency (about two times lower K_i values) was attained by subsequent substitutions of the central secondary amino group of the linker by small hydrophobic groups, e.g., the butyl moiety in **3** or *tert*-butyl (1,1-dimethylethyl) moiety in **5**. The addition of small substituents with a polar group (e.g., hydroxyethyl in **4** or carboxypropyl in **7**) had no significant effect on the K_i value. Interestingly, the addition of a bridged cobalt(III) bis (dicarbollide) substituent in **13** significantly improved the inhibitory efficiency (K_i values lowered 20 times compared to **1**).

The inhibition potency against resistant HIV PR variants was tested for selected competitive inhibitors from this series and seven HIV PR variants representing enzyme mutations for various FDA-approved protease inhibitors. Four of the HIV PR variants (PR1−4, Figure 1) used in the inhibition assay were prepared by site-directed mutagenesis, whereas three highly resistant HIV PR species (PR5−7, Figure 1) were amplified from HIV-positive patients failing antiretroviral therapy with HIV PR inhibitors. In Figure 1, the resistance profile for four compounds is expressed as a

Table 1. Structures and Inhibitory Constants of Metallacarborane Inhibitors of HIV-1 PR

General formula[a]			14[a]		
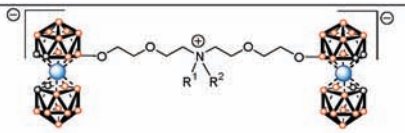			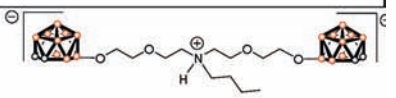		
Compound description			**in vitro enzyme assay**		
No.	***R*^{1}**	***R*^{2}**	***IC*$_{50}$**	***Mechanism***	***K*$_i$ *(nM)***
1	H	H	140 nM	competitive	4.9 ± 2.1
2			160 nM	concentration dependent[b]	N.D.
3		H	100 nM	competitive	2.2 ± 1.2
4		H	140 nM	competitive	4.7 ± 1.2
5		H	130 nM	competitive	2.7 ± 1.1
6	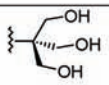	H	190 nM	noncompetitive	N.D.
7	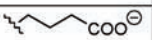	H	110 nM	competitive	4.2 ± 1.5
8	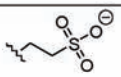	H	110 nM	noncompetitive	N.D.
9	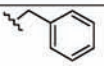	H	140 nM	concentration dependent[b]	N.D.
10	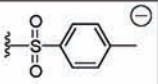	none	70 nM	concentration dependent[b]	N.D.
11[c]	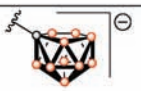	H	50 nM	noncompetitive	N.D.
12[c]	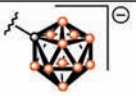	H	58 nM	concentration dependent[b]	N.D.
13[c]	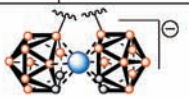		250 nM	competitive	0.27 ± 0.33
14	see Fig. above		8.5 μM	N.D.	N.D.

[a] Color coding: orange, BH groups or B (if substituted); black, CH groups or C (if substituted); blue, Co atom. [b] With the increasing concentration, the inhibition mechanism changes from noncompetitive through mixed toward competitive. [c] The carborane or metallacarborane cluster substituents are covalently bound to the central nitrogen atom of the linker in the case of compound **13** by a bridging manner.

vitality value representing a measure of the relative capacity of the mutated enzyme to cleave its substrate in the presence of an inhibitor.[18] For comparison, seven clinically used inhibitors (saquinavir, indinavir, nelfinavir, lopinavir, amprenavir, atazanavir, and darunavir) were included in our inhibition assay. Tested cobaltacarborane compounds show low relative loss of activity as indicated by low values of vitalities for all tested HIV-1 PR variants and proved thus to be specific inhibitors of the mutated HIV-1 PRs. Similar inhibition profiles were obtained previously for **3**, **1**, and other cobaltacarborane compounds and the molecular mechanism of inhibition potency toward PI-resistant HIV PR species was studied by molecular modeling.[14] Strikingly, the compound **13**, which shows the highest in vitro inhibitory efficiency, loses its potency against four of the tested HIV PR variants. The vitality values could not be determined for compound **13** and proteases PR6 and PR7 because the inhibitor concentration needed to inhibit these enzyme variants was above the compound solubility limit. This, however, indicates high resistance of PR6 and PR7 species against **13**. Interestingly, the comparison of values for PR2 and PR3 variants (differing only by the presence or absence of mutation M46I, respectively) shows 4.5-fold increase in vitality value for PR2. This suggests a role of residue 46 in compound **3** binding.

Crystal Structure. To gain structural information on binding of metallacarborane compounds containing two linked cobalt bis(1,2-dicarbollide) clusters to the HIV PR, we have determined the crystal structure of wild-type HIV-1 PR in complex with the parent compound of this series, the inhibitor **1**. Crystals of the complex exhibited the symmetry of orthorhombic space group *C*222 and contained one protease monomer in the asymmetric unit with a solvent content of 50%. The crystal structure was determined by molecular replacement and was refined using data to 1.7 Å resolution. The final model contains complete HIV-1 PR monomer (99 residues) and 23 non-hydrogen atoms of one cobalt bis(1,2-dicarbollide) cluster of the compound **1**. The biologically relevant unit, the HIV PR dimer, can be generated through crystal symmetry operations (rotation along 2-fold axis, Figure 2A). In addition to dimer, a crystallographic tetramer with two dimers arranged head-to-head by their active sites is also observed for this structure. This crystal packing was also present in previously determined crystal structure of HIV PR in complex with the parent cobalt bis(1,2-dicarbollide) ion (PDB code 1ZTZ[4]). The biological relevance of this crystallographic oligomer in solution, however, remains to be addressed by further studies.

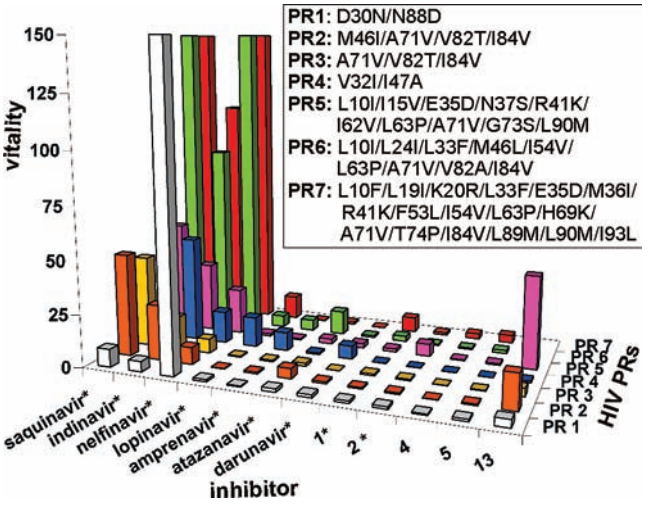

Figure 1. Vitality values of seven clinical inhibitors and five cobaltacarborane compounds analyzed with the panel of HIV-1 PR resistant species. Mutations in HIV-1 PR variants are shown in the figure inset. The vitality[18] is defined as $(K_i k_{cat}/K_m)_{MUT}/(K_i k_{cat}/K_m)_{WT}$, where MUT and WT are mutated and wild-type enzyme variant, respectively. The vitality values could not be determined for compound **13** and proteases PR6 and PR7 because the inhibitor concentration needed to inhibit these enzyme variants was above the compound solubility limit. Enzyme characteristics and K_i values are summarized in Tables S1 and S2 in Supporting Information. The asterisks mark data published in our previous work.[14]

Overall, the enzyme structure resembles the structure of an apoenzyme with open flap conformation rather then closed conformation typical for complexes with active-site inhibitors; however, the conformation of the flaps' tips (residues 47−55) is unique. The cobalt bis(1,2-dicarbollide) cluster of **1** could be modeled into well-defined electron density, however, no continuous map for the linker connecting the two cobalt bis(1,2-dicarbollide) clusters of **1** was observed (Figure 2B). This part is thus missing in the final crystallographic structure. The fact that the linker is disordered in the crystal structure of the PR:**1** complex suggests that it is inherently flexible and is able to adopt alternative conformations. To determine which of these **1** conformers would be energetically feasible in the enzyme cavity, we employed computational procedures.

Comparison of the HIV PR:**1** complex with the previously determined crystal structure of HIV PR in complex with the parent cobalt bis(1,2-dicarbollide) ion (PDB code 1ZTZ[4]) revealed an overall similar inhibitor binding mode but uncovered numerous differences in protein−inhibitor interactions. The overall deviation (rmsd) of the main-chain atoms of HIV PR dimers in **1** and cobalt bis(1,2-dicarbollide) ion complexes is 0.87 Å, suggesting that the inhibitor binding slightly alters the protein structure. Significant structural differences (with the rmsd values for main-chain atoms >0.7 Å[19]) are localized in the tip of flap residues 46−55 (Figure 3) and solvent exposed inherently flexible surface loop (residues 66−71).

In both crystal structures, the cobalt bis(1,2-dicarbollide) cluster occupies a hydrophobic pocket whose bottom is formed by enzyme residues Pro81, Val82, and Ile84 and is covered by the flap residues Ile47, Gly48, and Ile54. This site corresponds approximately to S3 and S3′ substrate-binding subsites. Two cobalt bis(1,2-dicarbollide) clusters bind to HIV PR dimer, and their binding blocks the closing of the two flexible flaps over the enzyme active site (Figure 3A).

While the HIV PR complex structure with parent cobalt bis(dicarbollide) ion shows an asymmetric binding of the two

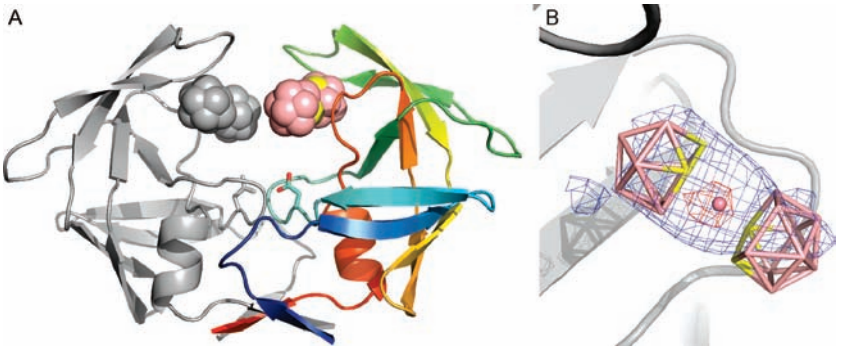

Figure 2. (A) Overall view of the crystal structure of the HIV PR:**1** complex. The HIV PR main-chain is represented as a cartoon with catalytic aspartates shown in sticks. Atoms of cobalt bis(1,2-dicarbollide) cluster of **1** are shown as spheres with boron and carbon atoms colored pink and yellow, respectively. One HIV PR monomer with cobalt bis(1,2-dicarbollide) cluster of **1** present in the crystal asymmetric unit is represented in rainbow coloring (N-terminus blue, C-terminus red), while gray colors represent the symmetrically related molecule. (B) Close view on the **1** cobalt bis(1,2-dicarbollide) cluster bound to HIV PR monomer with $F_o - F_c$ omit map contoured at 2.0σ (blue) and 8.0σ (red).

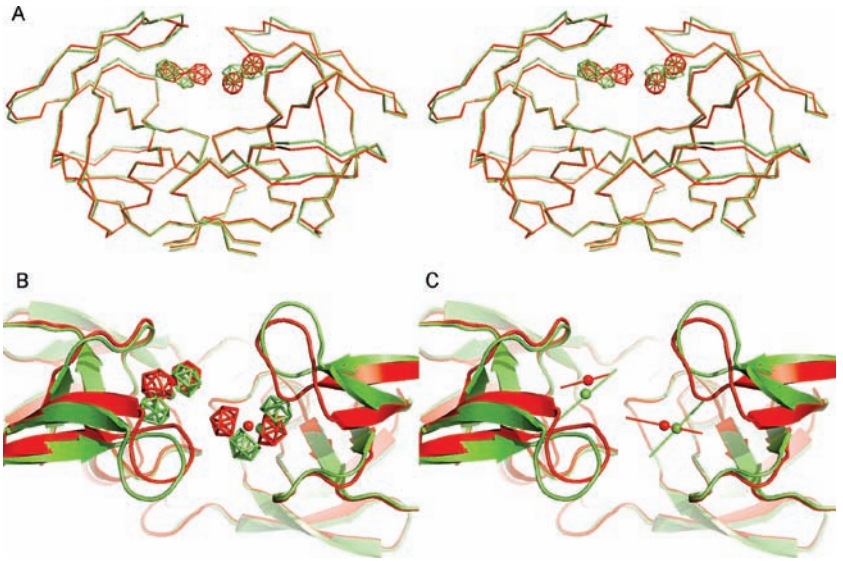

Figure 3. Comparison of cobalt bis(1,2-dicarbollide) ion and **1**:HIV-1 PR complex structures. (A) Stereo view of a superposition of the overall structures of HIV-1 PR with cobalt bis(dicarbollide) ion (PDB code 1ZTZ[4]) and **1** compounds, respectively, bound to the enzyme dimer. The enzyme is represented by its Cα trace, and cobaltacarboranes are shown as sticks. HIV PR:cobalt bis(1,2-dicarbollide) ion and HIV:**1** complexes are colored red and green, respectively. The linker connecting two cobaltacarborane clusters in **1** is disordered and thus missing in the crystallographic model. (B) Close-up top view into the enzyme active site showing differences in HIV PR:cobalt bis(1,2-dicarbollide) ion (red) and HIV PR:**1** (green) structures. Carbon and boron atoms in cobaltacarboranes are shown as sticks with central cobalt atom represented by a sphere. (C) Same view and color coding as in (B). Cobalt bis(1,2-dicarbollide) clusters are represented by their longitudinal axes with the central cobalt atom shown as a sphere.

cobalt bis(1,2-dicarbollide) clusters into two symmetrical binding sites present in the enzyme dimer, in the HIV PR:**1** complex, the two cobalt bis(1,2-dicarbollide) clusters of **1** occupy their binding sites symmetrically. The symmetry in binding of the two clusters of **1** into the symmetric protease dimer is also reflected in higher symmetry of the HIV PR:**1** crystals. The HIV PR:cobalt bis(dicarbollide) crystals belonged to the monoclinic space group *C*2 with one protease dimer related by noncrystallographic 2-fold axis in one asymmetric unit.[4] On the other hand, the HIV PR:**1** crystallized in the orthorhombic space group *C*222 with a crystallographic 2-fold axis relating the two protease monomers with bound metallacarborane cluster of **1**.

Although the inhibitor binding site is conserved in both complexes, the orientation of the parent metallacarborane cluster and **1** differ (Figure 3B). The clusters' central cobalt atoms in **1** are shifted by 1.5 and 1.3 Å compared to the corresponding atoms in parent bis(1,2-dicarbollide) cluster. Also, the **1** clusters are rotated by 37 and 44° with respect to the two clusters of bis(1,2-dicarbollide) ion. As a result of these cluster position rearrangements, the extent of interactions with individual protein residues differs. Compound **1** forms more interactions with flap residues (Ile 47, Gly 48, and Ile 54) than with the bottom of the binding site.

Binding Mode of the Linker in 1. Molecular modeling and calculations were employed to explore the conformational space of the inherently flexible linker of **1**. By use of molecular-dynamics based quenching technique (MD/Q) (for details, see Supporting Information), accessible conformations of the **1** linker within the HIV PR active site were computationally sampled. Quantum mechanics/molecular mechanics (QM/MM) optimizations for 20 snapshots from the MD/Q protocol resulted in a set of conformers differing substantially in energy (differences up to 40 kcal/mol). On the basis of a criterion of copopulation/interchangeability in the enzyme−inhibitor complex, we selected five lowest-energy structures differing in the linker conformation with an energy span of at most 3 kcal/mol (for a discussion of the energy cutoff, see ref 20). These five **1** conformers shared the common position of the central nitrogen atom of the linker secondary amino group. Interestingly, in the crystal structure, a spherical electron density is noticeable in the vicinity of this predicted nitrogen atom position (distance of 1.5−3.4 Å). This electron density was modeled in the crystal structure as a water molecule (W110). However, this electron density peak can also be explained by a common position of the central nitrogen atom shared by various conformations of the disordered linker. Further refinement of the models was therefore carried out using QM/MM calculations, where the central nitrogen atom was constrained to the position of the spherical electron density map yielding the final predicted linker conformations. Four resulting lowest-energy conformers fall within the range of 3 kcal/mol and are thus predicted to be copopulated in the complex structure (Figure 4A).

Discussion

In this study, we focused on substituted cobalt bis(dicarbollides) as specific inhibitors of HIV PR.[4] We explored the inhibition properties of compounds based on the parent formula $[H_2N\text{-}(8\text{-}(C_2H_4O)_2\text{-}1,2\text{-}C_2B_9H_{10})(1',2'\text{-}C_2B_9H_{11})\text{-}3,3'\text{-}Co)_2]Na$ (compound **1**, Table 1). In an attempt to map steric requirements of substituents at the central nitrogen atom as well as the influence of the hydrogen bonding potential on the activity of compounds, we focused on the substitution of the central part by a variety of groups differing in functionality/bulkiness/charge of the substituent. We used reactions on a cobalt bis(dicarbollide)(1−) cage (Scheme 1), based on Plesek's original synthetic concept,[21,22] which have recently become a versatile approach for incorporating metallaborane clusters into various functional molecules and materials (see Semioshkin et al., 2008, for a recent review[23]).

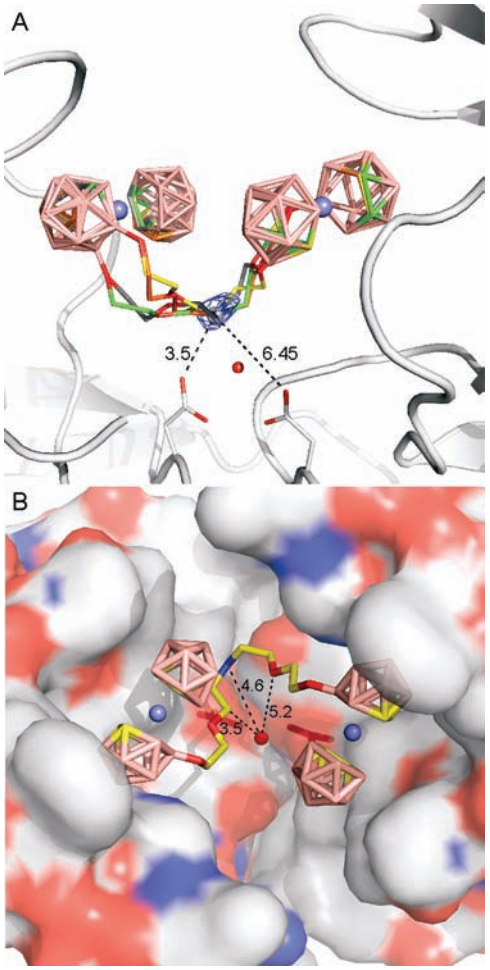

Figure 4. Molecular modeling of the **1** linker. (A) The four lowest-energy **1** conformers obtained from molecular modeling and calculations are represented by stick model with differentially colored carbon atoms and oxygen atoms in red. Boron and cobalt atoms are colored pink and blue, respectively. The $2F_o - F_c$ map modeled as a water molecule in the crystallographic model is shown at 1.0 σ. The position of this water molecule (shown as gray sphere) was used to fix the position of the nitrogen atom of the linker's central secondary amino group. The dashed lines and numbers represent the distances to catalytic aspartates (in Å), catalytic water is shown as a red sphere. (B) Top view into the HIV PR active site with the lowest energy model of the compound **1** linker. Protease is represented by its solvent accessible surface colored by the atom type (carbon gray, oxygen red, and nitrogen blue). The closest distances between linker atoms and the catalytic water (red sphere) are shown as dashed lines and numbers (in Å).

The in vitro inhibition assays proved their inhibition efficiency toward wild-type HIV PR as well as toward resistant variants. Strikingly, it also revealed various modes of inhibition for various compounds in our series: competitive, mixed, and noncompetitive.

The competitive mode of inhibition implies that the inhibitor competes with the substrate for binding to the enzyme active site. This mode of action is supported by previously published crystal structure of the parent bis(1,2-dicarbollide) ion[4] bound to the active site of HIV PR as well as by the crystal structure of compound **1**:enzyme complex presented in this work.

Mixed and noncompetitive types of inhibition might suggest specific binding of compounds outside the enzyme active site. The binding site most likely involves a functionally important part of the enzyme other than the active site, i.e., the dimerization interface or the flap region. A noncompetitive mode of inhibition might also be explained by the activity of inhibitor aggregates that bind outside of the enzyme active site cavity. The aggregation behavior of cobalt bis(dicarbollides) in solution was previously described and studied in detail.[24] Light scattering and atomic force microscopy techniques revealed that the behavior of aggregates of cobalt(III) bis(1,2-dicarbollide) compounds in aqueous solutions is fairly complex and depends on numerous factors, including compound concentration.[24,25] Interestingly, the formation of larger aggregates upon dilution of cobalt bis(dicarbollide) ion solutions was observed.[25] Indeed, for some compounds in this study, we observed concentration-dependent inhibition mode. For high compound concentration, the inhibition mechanism was distinctly competitive, while for low compound concentration, the transition to mixed and noncompetitive inhibition mechanism was obvious (Figure S1C3 in Supporting Information). Potential binding of the aggregates to the enzyme, however, must be tested experimentally and will be a subject of our further studies.

The X-ray structure of **1** bound to the wild-type HIV-1 PR is the second structure of this enzyme with bound metallacarborane in the active site. Although the linker part of **1** molecule is disordered in our crystal structures, the position of cobalt bis(1,2-dicarbollide) cluster and especially the position of the sandwiched cobalt atom was supported by well-defined electron density maps (Figure 2B). This map was used to model and refine one bis(1,2-dicarbollide) cluster to one enzyme monomer in the asymmetric unit. The average atomic displacement parameter (ADP) for the cluster atoms is higher by about 35% compared to the average ADP for the protein atoms (52 vs 38.2 Å), suggesting partial static or dynamic disorder of this part within the crystal. Comparison with our previous structure of HIV-1 PR in complex with parent cobalt bis(dicarbollide) ion[4] revealed that the metallacarborane cluster can acquire various positions within the common inhibitor binding site. Freedom in positions was indeed already proposed from modeling of parent cobalt bis(dicarbollide)(1−) binding into resistant protease species with mutations in S3 and S3′ substrate-binding subsites.[14]

Computational procedures helped us to model the position of the linker connecting two cobalt bis(1,2-dicarbollide) clusters of **1**. Because of the inherent flexibility of the linker of **1** within the HIV PR active site cavity, there is no continuous experimental electron density for the linker. The set of alternative models with similar energy shared a common position of the nitrogen atom of the linker's central secondary amino group, which is corroborated by the presence of electron density map peak in our crystal structure. The linker is placed asymmetrically within the symmetric cavity of the enzyme active site (with symmetrically bound metallacarborane clusters). The central nitrogen is within hydrogen bonding distance of 3.5 Å with one of the two catalytic aspartates (Figure 4A) and in a distance of 4.6 Å from the catalytic water (Figure 4B). Another possible hydrogen bonding partner is the main-chain carbonyl oxygen of Gly27 (distance 3.6 Å). The position of the linker in our model allows an opportunity for small substituents on the central amino group to be placed into the hydrophobic groove formed by Val82, Ile84, Leu10, and Leu23 (pointing "upwards" in Figure 4B) or even deeper into the dimeric interface and perhaps result in mixed inhibition by disrupting the active protease dimer. Another option for the substituent binding is to replace catalytic water and

occupy the polar pocket formed by the catalytic aspartate dyad (Figure 4B).

Our model can be used to propose potential binding mode of the compounds with the competitive mode of inhibition (Table 1). The nonpolar substituents of **2** and **5** could be accommodated in the hydrophobic pocket, and this interaction could account for the slight increase in their inhibition potency compared to compound **1**. To accommodate the *tert*-butyl moiety of **5** into the rather narrow hydrophobic groove structural rearrangements in PR would have to occur to achieve a productive binding conformation. The polar chains of **4** and **7** could fit well into the polar groove with a possibility of hydrogen bonding interactions to the catalytic aspartates. Our model is unable to explain binding of the compound **13**, as modeling of the bulky metallacarborane substituent produces sterical clashes with PR. Larger structural rearrangements in PR as well as in the compound **13** are needed for inhibitor binding. The binding mode of compound **13** probably differs substantially from the other substituent in our series. This is, indeed, indicated by the differential resistance profile of **13** (Figure 1) compared to other metallacarborane competitive inhibitors. To evaluate our hypotheses, the enzyme−inhibitor cocrystal structures are needed. However, our current models can be used in future compound optimization and design. Specifically, in our future design we will address the issue of optimal size and flexibility of the linker and also focus our optimization effort on improving physicochemical properties of the compounds to increase solubility and prevent aggregation.

In conclusion, our structure-based design led to the development of HIV PR inhibitors utilizing a novel boron-cage scaffold. Our X-ray structure analysis and modeling of a protein−inhibitor complex uncovered potentially important molecular interactions useful in the design of more potent inhibitors based on substituted cobalt bis(dicarbollides).

Experimental Procedures

Chemical Syntheses. Instrumental Methods Used for Compounds Characterization and Purity Check. A combination of instrumental methods was used for identification, characterization, and purity check of all compounds. The ^{1}H and ^{11}B and ^{13}C NMR spectra were recorded on Varian Mercury 400 Plus instrument. The spectral pattern and peak intensities corresponded to a particular structure and substitution pattern on each cluster molecule. Mass spectrometry measurements were carried out on a Thermo-Finnigan LCQ-Fleet ion trap instrument using electrospray ionization (ESI) in a negative mode. In most cases, negative ions corresponding to the molecular ion were observed with 100% abundance for the highest peak in the isotopic distribution plot. Molecular ions $[M]^-$ were detected for all univalent anions (compounds **1**−**6**, **9**, and **14**). $[M]^{2-}$ and $[M + H]^-$ or $[M + Na]^-$ ions were observed for the divalent anions (compounds **7**, **8**, and **10**−**13**). The isotopic distribution in the boron plot of $[M]^{2-}$ peaks was in agreement with the charge, showing distances of 1/2 mass units for dianionic compounds. Full agreement of the experimental and calculated isotopic distribution pattern was observed for all the compounds.

As previously verified, the data of elemental analyses of sodium salts of cobalt bis(dicarbollides) are often misleading due to variable content of water or other solvent molecules associated with the cation and cannot be considered as appropriate criterion of purity.[26] The identity of the reported compounds has been unambiguously proven by their spectral data and the purity assessed by analytical HPLC. A Merck-Hitachi HPLC system LaChrom 7000 series was used through the study employing an Ion-Pair RP chromatographic method with an isocratic elution based on the methods previously reported[27] for the separation of hydrophobic borate anions. The purity of all compounds, as determined by HPLC, was better than 98.0%.

Chemical Syntheses of Inhibitors (General Procedure). The synthesis of **1** and **3** was already reported in the previous paper along with the corresponding data for the compound's characterization.[4] The general methods for the synthesis of double-cluster cobalt bis (1,2-dicarbollide) compounds consisted from ring cleavage of the $[(8\text{-}O(C_2H_4)_2O\text{-}1,2\text{-}C_2B_9H_{10})\text{-}(1',2'\text{-}(C_2B_9H_{11})\text{-}3,3'\text{-}Co]^0$ (8-dioxane-**1**) by amines.

The starting cobalt bis(dicarbollide) building block (8-dioxane-1, 165 mg, 0. 40 mmol) was dissolved in toluene/DME (3:1, 10 mL) solvent mixture and stirred with the respective amine (0.41 mmol) in the same solvent (10 mL) at room temperature. The reaction course was monitored on TLC until the spot of the starting 8-dioxane-**1** disappeared. The intermediate products, i.e., the respective hydrogen 8-(XNH_2-3-oxa-pentoxy)-3-cobalt bis(1,2-dicarbollide)ate zwitterions were not isolated, but their solutions were directly stirred with NaH 22 mg (dry, 96%, 0.84 mmol) for 2 h. Then one additional equivalent of 8-dioxane-**1** (165 mg, 0.41 mmol) in toluene/DME solution (3:1 v/v, 10 mL) was added dropwise from a syringe and the reaction mixture was stirred 12−16 h at ambient temperature when the spot of 8-dioxane-**1** on TLC diminished. The reaction was quenched by careful addition of methanol (1 mL). Water was added (2 mL) and the resulting solution was neutralized with few drops of acetic acid (1.0 M), and solvents were removed in vacuum. The crude products were dissolved in Et_2O (25 mL) and shaken with water (2 × 20 mL). The organic layer was filtered, and the solvent was removed under reduced pressure. The purification of the crude product was accomplished by successive column chromatography over silica gel using CH_2Cl_2−CH_3CN mixture (1:4 to 1:3 v/v) as the mobile phase, eventually by crystallization from CH_2Cl_2 (with few drops of CH_3OH until dissolution) upon layering with hexane.

Representative examples of compound preparations and their spectral data are summarized below. For yields, NMR, MS, and other data were used for characterization of remaining compounds (see the Supporting Information).

Sodium Diethylimino Bis-8,8-[5-(3-oxa-pentoxy)-3-cobalt Bis-(1,2-dicarbollide)]diate (1−), $[(C_2H_5)_2N\text{-}(8\text{-}(C_2H_4O)_2\text{-}1,2\text{-}C_2B_9H_{10})(1',2'\text{-}C_2B_9H_{11})\text{-}3,3'\text{-}Co)_2]Na$, 2. Diethylamine was used for the ring cleavage. Yield 305 mg (83%); mp 268 °C (decomp.); TLC (acetonitrile/chloroform 1:2 v/v); R_F = 0.27 ($CHCl_3$:CH_3CN, 2:1); HPLC k' = 6.04; MS-ESI (m/z): 894.82 (100%) calcd 894.75, 899.78 (2%) $[M]^-$ calcd 999.73. ^{1}H $\{^{11}B\}$ NMR (400 MHz, acetone-d_6), [$^{1}H\{^{11}B_{selective}\}$ in square brackets]: δ 4.167 (s, 4H, CH_{carb}), 4.092 (s, 4H, CH_{carb}), 4.035 (br t, J = 4.0, 4H, OCH_2−CH_2O), 3.746 (t, J = 4.4, 4H, O-CH_2-CH_2O), 3.698 (q, J = 7.1, 4H, CH_3-CH_2-N), 3.627 (t, J = 4.6, 4H, OCH_2−CH_2O), 3.597 (m, J = 4.8, 4H, O-CH_2-CH_2-N), 1.418 (t, J = 7.2, 6H, CH_2-N); [2.92] (H10′), [2.79] (H8′), [2.71] (H4′,7′), [2.68] (H10), [2.95 s, 2.05 s, 1.84 s] (H 4, 7, 9, 12, 9′, 12′), [1.68] (H6′), [1.62] (H5′, 11′), [1.55] (H5, 11), [1.45] (H6). $^{13}C\{^{1}H\}$ NMR (100 MHz, acetone-d_6): δ 73.07 (CH_2−O), 69.75 (CH_2−O), 65.19 (CH_2−O), 56.2, 55.5 (CH_2−N), 54.23 (CH_{carb}), 47.45 (CH_{carb}), 19.91 (−CH_3). ^{11}B NMR (128 MHz, acetone-d_6): δ 23.89 (s, 2B, B8), 5.48 (d, J = 137, 2B, B8′), 0.42 (d, J = 150, 2B, B10′), −2.63 (d, J = 150, 2B, B10), −4.55 (d, J = 149, B4′,7′), −7.05 d, −7.67 (2d, overlap B9, 12, 9′, 12′), −17.30 (d, J = 159, 4B, B5′, 11′), −20.15 (d, J = 161, 4B, B5, 11), −22.25 (d, J = 158, 2B, B6′), −28.73 (d, J (B,H) = 140, 2B, B6).

Sodium Hydrogen 2-Hydroxyethylimino Bis-8,8-[5-(3-oxa-pentoxy)-3-cobalt Bis(1,2-dicarbollide)]diate (1−), $[(HOC_2H_4)\text{-}NH\text{-}(8\text{-}(C_2H_4O)_2\text{-}1,2\text{-}C_2B_9H_{10})(1',2'\text{-}C_2B_9H_{11})\text{-}3,3'\text{-}Co)_2]Na$, 4. Ethanolamine was used as the respective reagent. Yield of the sodium salt: 323 mg (89%). TLC ($CHCl_3$/CH_3CN 2:1 v/v) R_F = 0.22; HPLC k' = 3.37; MS 883.80 (100) (calc 883.71), m/z = 887.68 (2) $[M]^-$ (calc 887.68). ^{1}H $\{^{11}B\}$NMR [$^{1}H\{^{11}B_{selective}\}$ in square brackets], (400 MHz, acetone-d_6): δ 7.82 br s (2H, *NH*),

Table 2. X-ray Crystallography Statistics[a]

Data Collection Statistics	
space group	*C*222
cell parameters (Å)	58.16, 92.34, 48.95
wavelength (Å)	0.975
resolution (Å)	50−1.7 (1.76−1.7)
unique reflections	14821
redundancy	8.2 (5.9)
completeness (%)	95.4 (70.1)
R_{merge}[b]	4.9 (30.8)
average $I/\sigma(I)$	55.87 (4.3)
Wilson B (Å^2)	21.0
Refinement Statistics	
resolution range (Å)	23.8−1.7 (1.76−1.7)
no. of reflections in working set	13436 (694)
no. of reflections in test set	703 (30)
R value (%)[c]	17.6 (24.3)
R_{free} value (%)[d]	21.2 (29.5)
rmsd bond length (Å)	0.013
rmsd angle (deg)	3.76
no. of atoms in a.u.	945
protein atoms	806
ligand atoms	23
water molecules	111
mean B value (Å^2)	39.2
protein atoms ADP (Å^2)	38.2
inhibitor atoms ADP (Å^2)	52.1
solvent atoms ADP (Å^2)	45.7
Ramachandran plot	
residues in favored regions (%)	96.2
residues in allowed regions (%)	3.8

[a] The data in parentheses refer to the highest-resolution shell. ADP, atomic displacement parameter. [b] $R_{merge} = \sum_{hkl}\sum_i |I_i(hkl) - \langle I(hkl)\rangle| / \sum_{hkl}\sum_i I_i(hkl)$, where the $I_i(hkl)$ is an individual intensity of the ith observation of reflection hkl and $\langle I(hkl)\rangle$ is the average intensity of reflection hkl with summation over all data. [c] R value $= ||F_o| - |F_c|| / |F_o|$, where F_o and F_c are the observed and calculated structure factor amplitudes, respectively. [d] R_{free} is equivalent to R value but is calculated for 5% of the reflections chosen at random and omitted from the refinement process.[42]

4.158 s (4H, CH_{carb}), 4.095 s (4H, CH_{carb}), 3.94 t (8H, ^1J(H,H) = 5.6 Hz, O-CH_2-CH_2-O), 3.749 m (4H, O-CH_2-CH_2-O), 3.749 m (6H, O-CH_2-CH_2O; O-CH_2-CH_2N), 3.53 t (5 Hz, 2H, O-CH_2-CH_2N), [2.98] (H10′), [2.85] (H8′) [2.69] (H4′, 7′), [2.68] (H10), [2.95 s, 2.04 s, 1.84 s] (H 4, 7, 9, 12, 9′, 12′), [1.68] (H6′), [1.61] (H5′, 11′), [1.54] (H5, 11), [1.45] (H6). $^{13}C\{^1H\}$ NMR (100 MHz, acetone-d_6): δ 72.99 (CH_2-O), 69.73 (CH_2-O), 65.11 (CH_2-O), 56.31 (O-CH_2-CH_2-N), 54.65 (HO-CH_2-CH_2-N), 53.76 (CH_{carb}), 53.25 (HO-CH_2-CH_2-N), 47.44 (CH_{carb}). ^{11}B NMR (128 MHz, acetone-d_6): δ 24.01 (s, 2B, B8), 5.65 (d, 137 Hz, 2B, B8′), 0.42 (d, 142 Hz, 2B, B10′), −2.58 (d, 143 Hz, 2B, B10), −4.74 (d, 143 Hz, 4B, B4′, 7′) −7.00 (3d overlap, 12B, B4, 7, 9, 12, 9′, 12′), −17.28 (d, ^1J(B,H) = 156 Hz, 4B, B5′, 11′), −20.27 (d, 158 Hz, 4B, B5, 11), −22.22 (d, 173, Hz, 2B, B6′), −28.6 (d, 142 Hz, 2B, B6).

Sodium Hydrogen 3-Cobalt-bis(1,2-dicarbollid)-μ-8,8′-yl-imino-bis-8,8-[5-(3-oxa-pentoxy)-3-cobalt Bis(1,2-dicarbollide)]diate (2−), [(1″,2″-$C_2B_9H_{10}$)$_2$-3″-Co)-8″-μ-N-(8-(C_2H_4O)$_2$-1,2-$C_2B_9H_{10}$)(1′,2′-$C_2B_9H_{11}$)-3,3′-Co)$_2$]Na$_2$, 13. The [8,8′-μ-NH_2-(1,2-$C_2B_9H_{10}$)$_2$-3,3′-Co] bridge derivative[4] (135 mg, 0.40 mmol) was dissolved in toluene/DME (3:1, 15 mL) and treated with sodium hydride (22 mg, 0.84 mmol) under stirring for 2 h. Then solution of 8-dioxane-**1** (165 mg, 0.41 mmol) in toluene/DME (3:1, 15 mL) was injected. After stirring for 16 h, an additional portion of sodium hydride (11 mg, 0.42 mmol) was added, followed by dropwise addition of the second equivalent of 8-dioxane-**1** (165 mg, 0.41 mmol). The product was purified by chromatography and crystallization as described in general synthetic method above. Yield 215 mg (45%); mp 243 °C; TLC (acetonitrile/ chloroform 1:2 v/v) R_F = 0.20; HPLC k' = 2.20; MS 579.25 (100), m/z = 581.90 (8) $[M]^{2-}$ (calc 581.92), (4); 1180.88 (55), 1190.89 (1) $[M + Na]^-$ (calc 1190.88). $^1H\{^{11}B\}$ NMR (400 MHz, CD_3CN) [$^1H\{^{11}B_{selective}\}$ in square brackets]: δ 4.186 (s, 4H, CH_{carb}), 4.123 (s, 4H, CH_{carb}), 3.727 (t, J = 6.0, 4H, O-CH_2-CH_2O), 3.608 (s, 4H, CH_{carb}), 3.481 (t, J = 4.2, 4H, OCH_2−CH_2O), 3.399 (t, J = 4.3, 4H, O-CH_2-CH_2-O), 3.204 br. (s, 4H, O-CH_2-CH_2-N); [3.72, 3.49] (H4″, 7″, 9″, 12″), [3,4] (H10″], [2.79] (H10′), [2.606] (H10), [2.57] (H4′,7′), [2.42] (H8′), [2.78, 1.88 s, 1.62 s] (H 4, 7, 9, 12, 9′, 12′), [1.66] (H5″,11″), [1.62] (H6′), [1.57] (H5′, 11′), [1.54] (H6″), [1.47] (H5, 11), [1.45] (H6). $^{13}C\{^1H\}$ NMR, (100 MHz, CD_3CN): δ 72.90 (CH_2-O), 69.10 (CH_2-O), 65.30 (CH_2-O), 56.08 (CH_2-N), 54.93 (4C, CH_{carb}), 47.57 (8C, CH_{carb}). ^{11}B NMR (128 MHz, CD_3CN): δ 22.97 (s, 2B, B8), 9.64 (s, 2B, B8″), 3.74 (d, J = 138, 2B, B8′), −0.58 (d, J = 142, 2B, B10′), −0.85 (d, overlap, 2B, B10″), −2.65 (d, J = 153, 2B, B10), −4.81 (d, J = 144, 2B, B4′, 7′), −8.17 4 (d, overlap, 16B, B9, 12, 9′, 12′, 4″, 7″, 9″, 12″), 15.8 d (d, 2B, B5″, 11″), −17.44 (d, J = 153, 4B, B5′, 11′), −20.53 (d, J = 153, 4B, B5, 11), −21.8 (d, J = 164, 2B, B6′), −24.5 (br d, 2B, B6″), −28.43 (d, J = 162, 2B, B6).

Enzymes. For enzymatic assays, wild-type HIV-1 PR and its resistant variants were used. Resistant PRs were prepared by site-directed mutagenesis (HIV-1 PR 1−3) as described earlier[28] or selected under pressure of clinically used PIs (HIV-1 PR 4−6).[29] For crystallographic studies, HIV-1 PR variant bearing three mutations (Q7K, L33I, L63I) that minimize the autoproteolytic cleavage without changing other enzyme properties[30] was used. The expression, refolding, and purification of HIV-1 PR were performed as described previously.[28]

Enzymatic Assays. The inhibition analyses were performed by spectrophotometric assay using the chromogenic peptide substrate KARVNle*NphEANle-NH_2 as previously described.[28]

Substrate was added to final concentration near the K_m of the enzyme to 1 mL of 0.1 M sodium acetate buffer, pH 4.7, 0.3 M NaCl containing 6−8 pmol of PR and various concentrations of inhibitor dissolved in DMSO. The final concentrations of DMSO were kept below 2.5% (v/v). Substrate hydrolysis was followed as a decrease in absorbance at 305 nm using a UNICAM UV500 UV−vis spectrophotometer (Thermo, Cambridge, MA). The data were analyzed using the equation for competitive inhibition according to Williams and Morrison.[31] IC_{50} values were calculated for a given inhibitors by determining concentration needed to lower the initial HIV PR activity velocity to half using GraFt 5 software. The mechanism of inhibition was determined by Lineweaver−Burk plot.[17] Double reciprocal fits of initial rates versus concentration of substrate carried out at three fixed inhibitor concentrations were overlaid and yielded a pattern of lines characteristic of a particular mode of inhibition (Supporting Information).

Crystallographic Analysis. The complex for crystallization was prepared by mixing HIV-1 PR with 5-fold molar excess of compound **1** dissolved in DMSO. The complex was concentrated by ultrafiltration using Microcon-10 (Millipore) to concentration 7−9 mg/mL, and initial crystallization conditions were obtained by the vapor diffusion method in hanging drop mode using Wizard I and II crystallization screens (Emerald Biostructures). Optimal crystals were prepared by mixing 1 μL of protein at 7 mg/mL (in buffer contaning 50 mM sodium phosphate pH 6.5, 75 mM sodium chloride, 1 mM EDTA, 0.05% (v/v) β-mercaptoethanol, and 20% (v/v) glycerol) with 1 μL of reservoir solution (0.1 M *N*-cyclohexyl-3-aminopropanesulfonic acid (CAPS) pH 10.5, 1.2 M sodium dihydrogen phosphate, 0.2 M pottasium hydrogen phosphate, and 0.2 M lithium sulfate, final pH 6.0) and equilibration at 20 °C over 1 mL of reservoir solution.

Plate-like crystals grew to final size of 0.25 × 0.2 × 0.08 mm^3 within 3 days. For cryoprotection, the crystals were transferred into reservoir solution supplemented with 20% (v/v) ethylene

glycol, flash-cooled by plunging into liquid nitrogen and stored in liquid nitrogen until used for X-ray diffraction experiments.

Diffraction data were collected at 100 K at beamline 19-ID of the Structural Biology Center at the Advanced Photon Source, Argonne National Laboratory, Argonne, IL. Diffraction data were processed using the HKL-3000 suite of programs.[32] Crystal parameters and data collection statistics are given in Table 2.

The structure solution and refinement were performed using CCP4 program suite[33] graphical interface. HIV PR structure was solved by molecular replacement with the program MolRep[34] using protease monomer from Protein Data Bank structure 1ZTZ[4]. Initial $F_o - F_c$ difference Fourier map clearly showed presence of high positive maxima in the enzyme active cavity, indicating position of cobalt atom present in compound **1**. At this stage, the metallacarborane cluster of **1** was included into the model and the model was subjected to consecutive cycles of refinement using program Refmac5[35] and model building using program Coot.[36] The final steps included TLS refinement.[37] Atomic coordinates and experimental structure factors have been deposited with the Protein Data Bank with the code 3I8W. Refinement statistics is given in Table 2. The quality of the final model was validated with Molprobity.[38] All figures showing structural representations were prepared with the programs PyMOL.[39] The following services were used to analyze the structures: PISA server[40] and protein−protein interaction server.[41]

Molecular Modeling and Calculations. The structural model for the calculations was based on the PR:**1** crystal structure (this work). The linker was modeled connecting the two metal bis-(dicarbollide) cages. A computational screening of accessible conformations of the compound **1** linker was performed using a molecular dynamics based quenching technique (MD/Q) followed by quantum mechanics/molecular mechanics (QM/MM) optimizations. Details of this procedure are summarized in the Supporting Information.

Acknowledgment. We thank members of the Structural Biology Center at Argonne National Laboratory, the Advanced Photon Source, and Zbyszek Otwinowski (UT Southwestern Medical Center at Dallas) for their help with conducting X-ray data collection and Devon Maloy for critical proofreading of the manuscript. This work was supported by the European Commission sixth Framework no. LSHP-CT-2007-037693 and in part by the research projects nos. AV0Z50520514, AV0Z40320502, and AV0Z0550506 awarded by the Academy of Sciences of the Czech Republic, Grant IAAX00320901 from the Grant Agency of the Academy of Sciences of the Czech Republic, and LC512 and LC523 from the Ministry of Education of the Czech Republic. We are indebted to Praemium Academiae awarded to Pavel Hobza in 2007.

Supporting Information Available: List of mutations and enzyme characteristics [K_m, k_{cat}, and catalytic efficiencies (k_{cat}/K_m)] of PR variants analyzed in this study. K_i values [nM] for the inhibition of PR mutants by seven clinically available inhibitors and by metallacarboranes **1**, **3**, **4**, and **5**. The inhibition constants were determined by spectrophotometric assay at the pH optimum of the protease (pH 4.7). Examples of plots used for determination of inhibition mechanisms using double reciprocal Lineweaver−Burk plot. Competitive inhibition of **7**, noncompetitive inhibition **8**, inhibitor concentration dependent inhibition **12**. Experimental procedure on chemical syntheses and molecular modeling. This material is available free of charge via the Internet at http://pubs.acs.org.

References

(1) Kohl, N. E.; Emini, E. A.; Schleif, W. A.; Davis, L. J.; Heimbach, J. C.; Dixon, R. A.; Scolnick, E. M.; Sigal, I. S. Active human immunodeficiency virus protease is required for viral infectivity. *Proc. Natl. Acad. Sci. U.S.A* **1988**, *85*, 4686–4690.
(2) Mastrolorenzo, A.; Rusconi, S.; Scozzafava, A.; Barbaro, G.; Supuran, C. T. Inhibitors of HIV-1 protease: current state of the art 10 years after their introduction. From antiretroviral drugs to antifungal, antibacterial and antitumor agents based on aspartic protease inhibitors. *Curr. Med. Chem.* **2007**, *14*, 2734–2748.
(3) Condra, J. H.; Schleif, W. A.; Blahy, O. M.; Gabryelski, L. J.; Graham, D. J.; Quintero, J. C.; Rhodes, A.; Robbins, H. L.; Roth, E.; Shivaprakash, M.; et al. In vivo emergence of HIV-1 variants resistant to multiple protease inhibitors. *Nature* **1995**, *374*, 569–571.
(4) Cigler, P.; Kozisek, M.; Rezacova, P.; Brynda, J.; Otwinowski, Z.; Pokorna, J.; Plesek, J.; Gruner, B.; Doleckova-Maresova, L.; Masa, M.; Sedlacek, J.; Bodem, J.; Krausslich, H. G.; Kral, V.; Konvalinka, J. From nonpeptide toward noncarbon protease inhibitors: metallacarboranes as specific and potent inhibitors of HIV protease. *Proc. Natl. Acad. Sci. U.S.A* **2005**, *102*, 15394–15399.
(5) Grimes, R. N. Metallacarboranes in the new millennium. *Coord. Chem. Rev.* **2000**, *200*, 773–811.
(6) King, R. B. Three-dimensional aromaticity in polyhedral boranes and related molecules. *Chem. Rev.* **2001**, *101*, 1119–1152.
(7) Chen, Z. F.; King, R. B. Spherical aromaticity: Recent work on fullerenes, polyhedral boranes, and related structures. *Chem. Rev.* **2005**, *105*, 3613–3642.
(8) Lesnikowski, Z. J.; Paradowska, E.; Olejniczak, A. B.; Studzinska, M.; Seekamp, P.; Schussler, U.; Gabel, D.; Schinazi, R. F.; Plesek, J. Towards new boron carriers for boron neutron capture therapy: metallacarboranes and their nucleoside conjugates. *Bioorg. Med. Chem.* **2005**, *13*, 4168–4175.
(9) Sivaev, I. B.; Bregadze, V. V. Polyhedral Boranes for Medical Applications: Current Status and Perspectives. *Eur. J. Inorg. Chem.* **2009**, 1433–1450.
(10) Plesek, J. Potential Applications of the Boron Cluster Compounds. *Chem. Rev.* **1992**, *92*, 269–278.
(11) Olejniczak, A. B.; Plesek, J.; Kriz, O.; Lesnikowski, Z. J. A nucleoside conjugate containing a metallacarborane group and its incorporation into a DNA oligonucleotide. *Angew. Chem., Int. Ed.* **2003**, *42*, 5740–5743.
(12) Beatty, B. G.; Paxton, R. J.; Hawthorne, M. F.; Williams, L. E.; Rickard-Dickson, K. J.; Do, T.; Shively, J. E.; Beatty, J. D. Pharmacokinetics of an anti-carcinoembryonic antigen monoclonal antibody conjugated to a bifunctional transition metal carborane complex (venus flytrap cluster) in tumor-bearing mice. *J. Nucl. Med.* **1993**, *34*, 1294–1302.
(13) Paxton, R. J.; Beatty, B. G.; Hawthorne, M. F.; Varadarajan, A.; Williams, L. E.; Curtis, F. L.; Knobler, C. B.; Beatty, J. D.; Shively, J. E. A transition metal complex (Venus flytrap cluster) for radioimmunodetection and radioimmunotherapy. *Proc. Natl. Acad. Sci. U.S.A.* **1991**, *88*, 3387–3391.
(14) Kozisek, M.; Cigler, P.; Lepsik, M.; Fanfrlik, J.; Rezacova, P.; Brynda, J.; Pokorna, J.; Plesek, J.; Gruner, B.; Grantz Saskova, K.; Vaclavikova, J.; Kral, V.; Konvalinka, J. Inorganic polyhedral metallacarborane inhibitors of HIV protease: a new approach to overcoming antiviral resistance. *J. Med. Chem.* **2008**, *51*, 4839–4843.
(15) Plesek, J.; Jelinek, T.; Mares, F.; Hermanek, S. Unique Dialkylsulfonio-Methylation of the 7,8-$C_2B_9H_{12}(-)$ Ion to the 9-R2s-Ch2−7,8-C2b9h11 Zwitterions by Formaldehyde and Dialkyl Sulfides—General Synthesis of the Compounds 10-R2e-7,8-C2b9h11 (E═O,S). *Collect. Czech. Chem. Commun.* **1993**, *58*, 1534–1547.
(16) Stogniy, M. Y.; Abramova, E. N.; Lobanova, I. A.; Sivaev, I. B.; Bragin, V. I.; Petrovskii, P. V.; Tsupreva, V. N.; Sorokina, O. V.; Bregadze, V. I. Synthesis of functional derivatives of 7,8-dicarba-*nido*-undecaborate anion by ring-opening of its cyclic oxonium derivatives. *Collect. Czech. Chem. Commun.* **2007**, *72*, 1676–1688.
(17) Lineweaver, H.; D., B. The determination of enzyme dissociation constants. *J. Am. Chem. Soc.* **1934**, *56*, 656–666.
(18) Gulnik, S. V.; Suvorov, L. I.; Liu, B.; Yu, B.; Anderson, B.; Mitsuya, H.; Erickson, J. W. Kinetic characterization and cross-resistance patterns of HIV-1 protease mutants selected under drug pressure. *Biochemistry* **1995**, *34*, 9282–9287.
(19) Betts, M. J.; Sternberg, M. J. E. An analysis of conformational changes on protein−protein association: implications for predictive docking. *Protein Eng.* **1999**, *12*, 271–283.
(20) Fanfrlik, J.; Brynda, J.; Rezac, J.; Hobza, P.; Lepsik, M. Interpretation of protein/ligand crystal structure using QM/MM calculations: case of HIV-1 protease/metallacarborane complex. *J. Phys. Chem. B* **2008**, *112*, 15094–15102.
(21) Selucky, P.; Plesek, J.; Rais, J.; Kyrs, M.; Kadlecova, L. Extraction of Fission-Products into Nitrobenzene with Dicobalt Tris-Dicarbollide

and Ethyleneoxy-Substituted Cobalt Bis-Dicarbollide. *J. Radioanal. Nucl. Chem.* **1991**, *149*, 131–140.
(22) Plesek, J.; Hermanek, S.; Franken, A.; Cisarova, I.; Nachtigal, C. Dimethyl sulfate induced nucleophilic substitution of the [bis(1,2-dicarbollido)-3-cobalt(1−)]ate ion. Syntheses, properties and structures of its 8,8'-mu-sulfato, 8-phenyl and 8-dioxane derivatives. *Collect. Czech. Chem. Commun.* **1997**, *62*, 47–56.
(23) Semioshkin, A. A.; Sivaev, I. B.; Bregadze, V. I. Cyclic oxonium derivatives of polyhedral boron hydrides and their synthetic applications. *Dalton Trans.* **2008**, 977–992.
(24) Kubat, P.; Lang, K.; Cigler, P.; Kozisek, M.; Matejicek, P.; Janda, P.; Zelinger, Z.; Prochazka, K.; Kral, V. Tetraphenylporphyrin-cobalt(III) bis(1,2-dicarbollide) conjugates: from the solution characteristics to inhibition of HIV protease. *J. Phys. Chem. B* **2007**, *111*, 4539–4546.
(25) Matejicek, P.; Cigler, P.; Prochazka, K.; Kral, V. Molecular assembly of metallacarboranes in water: light scattering and microscopy study. *Langmuir* **2006**, *22*, 575–581.
(26) Gruner, B.; Mikulasek, L.; Baca, J.; Cisarova, I.; Bohmer, V.; Danila, C.; Reinoso-Garcia, M. M.; Verboom, W.; Reinhoudt, D. N.; Casnati, A.; Ungaro, R. Cobalt bis(dicarbollides)(1−) covalently attached to the calix[4]arene platform: The first combination of organic bowl-shaped matrices and inorganic metallaborane cluster anions. *Eur. J. Org. Chem.* **2005**, 2022–2039.
(27) Gruner, B.; Plzák, Z. *J. Chromatogr., A* **1997**, *789*, 497–517.
(28) Weber, J.; Mesters, J. R.; Lepsik, M.; Prejdova, J.; Svec, M.; Sponarova, J.; Mlcochova, P.; Skalicka, K.; Strisovsky, K.; Uhlikova, T.; Soucek, M.; Machala, L.; Stankova, M.; Vondrasek, J.; Klimkait, T.; Kraeusslich, H. G.; Hilgenfeld, R.; Konvalinka, J. Unusual binding mode of an HIV-1 protease inhibitor explains its potency against multi-drug-resistant virus strains. *J. Mol. Biol.* **2002**, *324*, 739–754.
(29) Vaclavikova, J.; Weber, J.; Machala, L.; Reinis, M.; Linka, M.; Bruckova, M.; Vandasova, J.; Stankova, M.; Konvalinka, J. Long-term analysis of the resistance development in HIV-1 positive patients treated with protease and reverse transcriptase inhibitors: correlation of the genotype and disease progression. *Acta Virol.* **2005**, *49*, 29–36.
(30) Mildner, A. M.; Rothrock, D. J.; Leone, J. W.; Bannow, C. A.; Lull, J. M.; Reardon, I. M.; Sarcich, J. L.; Howe, W. J.; Tomich, C. S.; Smith, C. W.; et al. The HIV-1 protease as enzyme and substrate: mutagenesis of autolysis sites and generation of a stable mutant with retained kinetic properties. *Biochemistry* **1994**, *33*, 9405–9413.
(31) Williams, J. W.; Morrison, J. F. The kinetics of reversible tight-binding inhibition. *Methods Enzymol.* **1979**, *63*, 437–467.
(32) Minor, W.; Cymborowski, M.; Otwinowski, Z.; Chruszcz, M. HKL-3000: the integration of data reduction and structure solution—from diffraction images to an initial model in minutes. *Acta Crystallogr., Sect. D: Biol. Crystallogr.* **2006**, *62*, 859–866.
(33) CCP4. The CCP4 suite: programs for protein crystallography. *Acta Crystallogr., Sect. D: Biol. Crystallogr.* **1994**, *50*, 760−763.
(34) Vagin, A.; Teplyakov, A. An approach to multi-copy search in molecular replacement. *Acta Crystallogr., Sect. D: Biol. Crystallogr.* **2000**, *56*, 1622–1624.
(35) Murshudov, G. N.; Vagin, A. A.; Dodson, E. J. Refinement of macromolecular structures by the maximum-likelihood method. *Acta Crystallogr., Sect. D: Biol. Crystallogr.* **1997**, *53*, 240–255.
(36) Emsley, P.; Cowtan, K. Coot: model-building tools for molecular graphics. *Acta Crystallogr., Sect. D: Biol. Crystallogr.* **2004**, *60*, 2126–2132.
(37) Winn, M. D.; Isupov, M. N.; Murshudov, G. N. Use of TLS parameters to model anisotropic displacements in macromolecular refinement. *Acta Crystallogr., Sect. D: Biol. Crystallogr.* **2001**, *57*, 122–133.
(38) Lovell, S. C.; Davis, I. W.; Arendall, W. B., III; de Bakker, P. I.; Word, J. M.; Prisant, M. G.; Richardson, J. S.; Richardson, D. C. Structure validation by Calpha geometry: phi,psi and Cbeta deviation. *Proteins* **2003**, *50*, 437–450.
(39) De Lano, W. L. *The PyMOL Molecular Graphics System*; DeLano Scientific LLC: San Carlos, CA; http://www.pymol.org.
(40) Krissinel, E.; Henrick, K. Detection of Protein Assemblies in Crystals. In *CompLife 2005, LNBI 3695*; Springer-Verlag: Berlin Heidelberg, 2005; pp 163−174.
(41) Jones, D. T.; Taylor, W. R.; Thorton, J. M. A Model Recognition Approach to the Prediction of All-Helical Membrane-Protein Structure and Topology. *Biochemistry* **1994**, *33*, 3038–3049.
(42) Brunger, A. T. Free *R*-Value—A Novel Statistical Quantity for Assessing the Accuracy of Crystal Structures. *Nature* **1992**, *355*, 472–475.